The Late Fall Extratropical Response to ENSO: Sensitivity to Coupling and Convection in the Tropical West Pacific

Ileana Bladé

Departament d'Astronomia i Meteorologia, Universitat de Barcelona, Barcelona, Spain

Matthew Newman

CIRES Climate Diagnostics Center, University of Colorado, and Physical Sciences Division, NOAA/Earth System Research Laboratory, Boulder, Colorado

Michael A. Alexander

Physical Sciences Division, NOAA/Earth System Research Laboratory, Boulder, Colorado

James D. Scott

CIRES Climate Diagnostics Center, University of Colorado, and Physical Sciences Division, NOAA/Earth System Research Laboratory, Boulder, Colorado

(Manuscript received 28 July 2006, in final form 11 March 2008)

ABSTRACT

The extratropical response to El Niño in late fall departs considerably from the canonical El Niño signal. Observational analysis suggests that this response is modulated by anomalous forcing in the tropical west Pacific (TWP), so that a strong fall El Niño teleconnection is more likely when warm SST conditions and/or enhanced convection prevail in the TWP. While these TWP SST anomalies may arise from noise and/or long-term variability, they may also be generated by differences between El Niño events, through variations in the tropical "atmospheric bridge." This bridge typically drives subsidence west of the date line and enhanced trade winds over the far TWP, which cool the ocean. In late fall, however, some relatively weaker and/or more eastward-shifted El Niño events produce a correspondingly weakened and displaced tropical bridge, which results in no surface cooling and enhanced convection in the TWP. Because the North Pacific circulation is very sensitive to forcing from the TWP at this time of year, the final outcome is a strong extratropical El Niño teleconnection.

This hypothesis is partly supported by regionally coupled ensemble GCM simulations for the 1950–99 period, in which prescribed observed El Niño SST anomalies in the eastern/central equatorial Pacific and an oceanic mixed layer model elsewhere coexist, so that the TWP is allowed to interact with the El Niño atmospheric bridge. To separate the deterministic signal driven by TWP coupling from that associated with inter–El Niño differences and from the "noise" due to intrinsic TWP convection variability (*not* induced by local SST anomalies), a second large-ensemble (100) simulation of the 1997/98 El Niño event, with coupling limited to the TWP and tropical Indian Ocean, is carried out. Together, the model findings suggest that the extratropical El Niño teleconnection during late fall is very sensitive to convective forcing in the TWP and that coupling-induced warming in the TWP may enhance this El Niño teleconnection by promoting convection in this critical TWP region. A more general implication is that diagnostic studies using December–February (DJF) seasonal averages may obscure some important aspects of climate anomalies associated with forcing in the tropical Pacific.

Corresponding author address: Dr. Ileana Bladé, Departament d'Astronomia i Meteorologia, Facultat de Fisica, Universitat de Barcelona, Av. Diagonal 647, 08028 Barcelona, Spain.
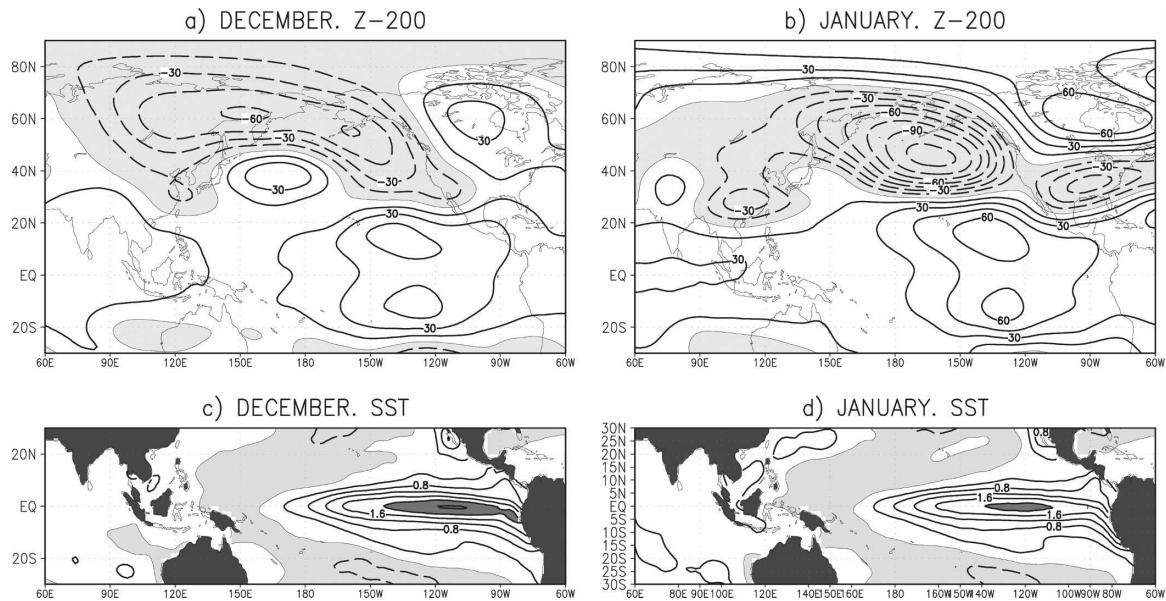E-mail: ileanablade@ub.edu

FIG. 1. Observed December and January composite anomalies of 200-hPa geopotential height and SST for nine moderate-to-strong El Niño events that occurred during the period 1950–99 (1957/58, 1965/66, 1969/70, 1972/73, 1976/77, 1982/83, 1987/88, 1991/92, and 1997/98). The anomalies are computed relative to the 1950–99 climatology. Contour interval is 15 m for geopotential height and 0.4 K for SST. Negative contours are lightly shaded. SST anomalies greater than 2 K are shaded in dark gray. The thin line is the zero contour.

1. Introduction

One surprising feature of the extratropical response to El Niño in the Northern Hemisphere (NH) is that it does not get completely established until January, even though the abnormal warming of the tropical eastern Pacific usually peaks during late fall. This might appear to conflict with the canonical model of El Niño, in which a warm SST anomaly in the central tropical Pacific generates a widespread region of stronger-than-normal convection east of the date line that consequently forces a wave train propagating across the Pacific and North America. In reality, and despite composite El Niño SST anomalies that are slightly stronger in December than in January (Figs. 1c,d), it is not until January that the composite El Niño geopotential height anomaly exhibits the well-known tropical Northern Hemisphere (TNH) teleconnection pattern (Mo and Livezey 1986) emanating out of the central equatorial Pacific (Fig. 1b). In contrast, the composite December wave train (Fig. 1a) has weaker amplitude and exhibits a different shape, with a trajectory that appears to originate in the western tropical Pacific (removing the zonal mean makes this source region even clearer). A similar distinction can be drawn using November–December (ND) and January–February (JF) averages (not shown). The tropical circulation anomalies (e.g., the pair of anticyclones straddling the equator) are also slightly stronger in January than in December, but this

difference is so minor that it seems unlikely to explain the extratropical differences. The contrast between the December and January El Niño wave trains is not a new result (e.g., Livezey et al., Wang and Fu 2000); yet, awareness of this large change in the El Niño teleconnection from late fall to winter is not widespread, as attested to by the large number of studies combining December and January extratropical anomalies into a seasonal December–February (DJF) winter anomaly.

The changing propagation path of the El Niño wave train suggests that its primary source shifts from the *western* tropical Pacific in late fall to the *central* tropical Pacific in winter. Several observational studies have indicated that SST and/or convective anomalies in the tropical western Pacific (TWP) play an important role in forcing the El Niño teleconnection, but the issue of whether this impact may vary with the annual cycle has not been addressed. For example, Hamilton (1988) found that SSTs in the TWP were a major factor in determining the winter NH atmospheric response to El Niño, with the response being most pronounced when the far western Pacific is anomalously warm (or at least not overly cold). Palmer and Owen (1986) suggest that enhanced rainfall over the tropical and subtropical western Pacific can produce a Pacific–North America (PNA)-like response, while Chen (2002) identified a short-wave train emanating from the TWP embedded within the large-scale El Niño teleconnection pattern. These results are supported by modeling experiments

indicating that SST and diabatic heating anomalies in the TWP can excite Rossby wave trains propagating into the North Pacific (Simmons et al. 1983; Palmer and Owen 1986; Barsugli and Sardeshmukh 2002; Hoerling and Kumar 2003; Quan et al. 2006; Lau et al. 2006), but again, none of these studies examined the seasonal dependence of this effect.

In this paper, we provide observational and modeling evidence that suggests that the extratropical response to El Niño *in late fall* is modulated by anomalous forcing in the TWP, so that a more prominent teleconnection occurs when warm SST conditions and/or enhanced convection prevail in the TWP. An important question then arises: Could these SST anomalies in the TWP be driven by the El Niño event itself rather than reflect random noise and/or decadal signals? Clearly, SST anomalies in the TWP can be generated by local oceanic processes unrelated to ENSO, and there have been studies suggesting some long-term (possibly multidecadal) variability in this region (Hoerling and Kumar 2003; Deser et al. 2004; Lau et al. 2006; Newman 2007). On the other hand, El Niño events themselves can induce SST anomalies in the TWP through a tropical "atmospheric bridge" that involves longitudinal shifts in the regions of deep convection and in the Walker circulation (Klein et al.1999; Lau and Nath 2003, hereafter LN03). During warm events, this bridge typically drives subsidence west of the date line and enhanced trade winds over the far TWP that cool the ocean, further inhibiting convection. It is thus plausible that interevent variations in the strength of this bridge could lead to interevent variations in the state of the TWP and in the associated extratropical response.

Whether the link between the TWP and the extratropical El Niño response is deterministically connected to El Niño (the TWP responds to the weak bridge and then drives a teleconnection to the North Pacific), a mere by-product of the perturbed tropical bridge (TWP is passive), or unrelated to ENSO (random SST variations in the TWP) cannot be answered solely on the basis of observations. Nor can it be diagnosed using a GCM forced with globally prescribed observed SSTs—for unless air–sea coupling is included, one cannot determine the role of the TWP *response* in mediating the changes to the extratropical El Niño teleconnection. A more suitable modeling strategy to investigate cause and effect is to prescribe observed SST forcing in the tropical eastern Pacific but elsewhere to allow the atmosphere to interact with a mixed layer model of the ocean, following the approach originally devised by Alexander (1992a,b) and used in many studies since (e.g., Bladé 1999; Alexander et al. 2002, hereafter A02; LN03; Huang et al. 2005; Seager 2007). These so-called

pacemaker experiments (Kinter et al. 2006) allow the El Niño response to be modulated by air–sea coupling and SST forcing in the TWP. Furthermore, by performing parallel uncoupled simulations in which the mixed layer is replaced by climatological SSTs, we may also be able to rule out a by-product response of the TWP to differences in the El Niño tropical bridge (since then the extratropical response would tend to be the same in the coupled and uncoupled experiments). Additionally, to separate the signal driven by coupling in the TWP from the signal associated with inter–El Niño differences and to isolate the impact of (random) convection in the TWP region, we analyze a large ensemble (100) of simulations of a single strong El Niño event (the 1997/98 episode).

The paper is organized as follows: after a description of the observational data, model, and experiments (section 2), we examine the fall-to-winter changes in the sensitivity of the observed North Pacific circulation to tropical forcing and we investigate the impact of the TWP on the late fall El Niño teleconnection during the period 1950–99 (section 3). We then repeat the analysis using data from the coupled GCM simulations (section 4) and also consider the deterministic impact of coupling in a large-ensemble single-event El Niño simulation (section 5). Conclusions and implications of the results are presented in section 6.

2. Data, model, and experiments used in this study

The observational data used in this paper are National Oceanic and Atmospheric Administration (NOAA) extended SST (Smith and Reynolds 2004), National Centers for Environmental Prediction (NCEP)–National Center for Atmospheric Research (NCAR) reanalysis geopotential height, sea level pressure (SLP) and surface zonal wind, and land-based rain gauge precipitation data from the Global Historical Climate Network (GHCN; Vose et al. 1992), inverse-distance weighted and averaged into $5° \times 5°$ grid boxes (J. Escheid 2006, personal communication), for the period 1950–99 as well as for the month of December 2006 (Fig. 12). All data are converted to monthly mean anomalies by removing the 50-yr (1950–99) mean for each month.

All experiments in this study are conducted with the Geophysical Fluid Dynamics Laboratory (GFDL) R30 AGCM, which has an equivalent resolution of $\sim 2.25°$ latitude by $3.75°$ longitude and 14 vertical sigma levels. For a description of the model and its climate, the reader is referred to Gordon and Stern (1982), Broccoli and Manabe (1992), and Alexander and Scott (1995). To study the impact of air–sea coupling in the TWP on

TABLE 1. Description of experiments.*

Experiment name	Period	Number of simulations	SST field in tropical eastern Pacific	Coupling configuration
CTRL	1950–99	8	Observed	No coupling
MLM	1950–99	16	Observed	Coupling in entire ice-free oceanic domain (except prescribed box in eastern tropical Pacific)
NEUTRAL	1996–99	150	"Climatological"	No coupling
CTRL	1996–99	150	Observed	No coupling
TROPMLM	1996–99	100	Observed	Coupling in tropical Indian and western Pacific Oceans only

* The NEUTRAL experiment is only used to provide a basic state against which to compute El Niño anomalies in the "short" TROPMLM and CTRL experiments. In all experiments (except for NEUTRAL) observed SSTs are prescribed in the tropical eastern Pacific box defined by 15°S–15°N, 172°E–South American coast (see box in Fig. 8e). "Climatological" SSTs are prescribed in the uncoupled regions of TROPMLM and CTRL (outside the tropical eastern Pacific) and in the entire domain in the NEUTRAL experiment (see text for more information).

the El Niño response, we performed coupled pacemaker experiments, in which SSTs in the tropical eastern Pacific (15°S–15°N, 172°E–South American coast, see box in Fig. 8e) are prescribed to evolve according to observations, but air–sea interactions may be allowed elsewhere. Two sets of coupled simulations were analyzed:

- MLM experiment: a relatively small (16 members) ensemble of globally coupled integrations for the period 1950–99, which has already been used in previous studies (A02; LN03). At each oceanic grid point outside the specified tropical eastern Pacific region (box in Fig. 8e), the atmosphere is coupled to a one-column entraining mixed layer ocean model.[1]
- TROPMLM experiment: a new "super-ensemble" (100 members) simulation of the 1997/98 El Niño event (starting in January 1996 and ending in December 1999), in which the interactive mixed layer ocean is restricted to the tropical Indian and western Pacific Oceans (between 15°S and 15°N). "Climatological" SSTs (see below) are specified elsewhere (outside the prescribed SST region).

For each set of experiments, a corresponding uncoupled control simulation, in which model "climatological" SSTs are specified at all oceanic grid points (outside the prescribed SST region), is also performed. For the TROPMLM simulations, a NEUTRAL experiment with climatological SSTs prescribed over the entire oceanic domain is also required to provide a basic state against which to compute anomalies (for the

MLM run, the anomalies are computed relative to its ensemble-mean long-term mean). The experiments consist of realizations initiated from different atmospheric conditions taken from a different simulation. The characteristics of each experiment are summarized in Table 1.[2]

The mixed layer model has been extensively documented in Alexander et al. (2000, A02). It simulates mixed layer temperature (or SST), salinity, and depth, and it includes local atmosphere–ocean fluxes, penetrating solar radiation, turbulent entrainment of water into the mixed layer, and diffusion. Because of the absence of ocean currents, surface heat and salt flux corrections are required to maintain the oceanic seasonal cycle close to observations. Small biases in SST ($<1°$C), however, still occur in the long-term monthly means at a few locations after the corrections are applied. Thus, for both long and short sets of integrations, a globally coupled MLM-type experiment is performed first, and its ensemble-mean long-term mean daily SSTs are used as the "climatological" SSTs in the remaining experiments. This ensures that within each set, all experiments share the same basic state and can be compared with each other. Important physical processes such as Ekman forcing, oceanic Rossby waves, and the Indonesian Throughflow are missing from the coupled ex-

---

[1] Oceanic grid points at which ice is present at any time in winter are treated identically in all simulations: sea ice (winter) or SST (summer), if applicable, is prescribed to repeat the observed climatological cycle. Hereafter "oceanic" refers to ice-free grid points.

[2] While the original MLM ensembles were run at GFDL, the new superensembles were run at ESRL. Compiler differences resulted in some differences in the mean climate and monthly variability, as assessed by comparing the GFDL MLM runs to an identical set run on the ESRL computers. These discrepancies are notable primarily at high latitudes, but for El Niño height composites they can amount to 20 m over the North Pacific. To be consistent with A02, all MLM results reported here use the GFDL simulations. The compiler differences have no qualitative impact on any of our results.
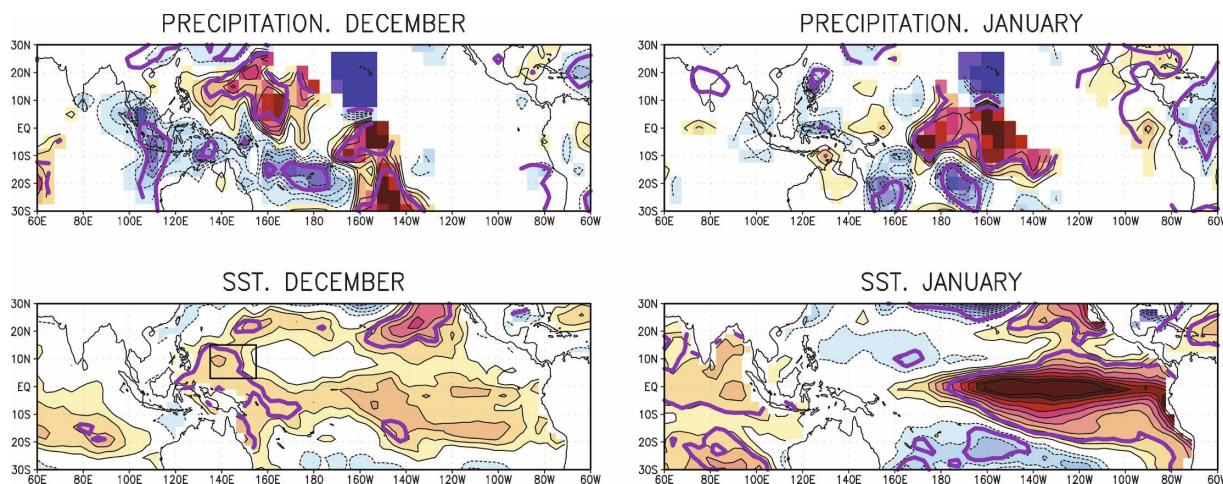
FIG. 2. (top) Observed regressions of (left) December and (right) January monthly precipitation against the NPI (Trenberth and Hurrell 1994) for the period 1950–99. Contour interval is 0.005 cm day^{-1}. Red/yellow (blue) shadings indicate positive (negative) values. The NPI is a measure of the strength of the Aleutian low (area-weighted sea level pressure over the region 30°–65°N, 160°E-140°W), with a std dev of 3.5 hPa in December and 4.4 hPa in January, and its sign has been reversed. (bottom) Same as (top), but for SST; contour interval is 0.01 K. The datasets employed are gridded GHCN precipitation (land-based rain gauge station data, averaged into 5° × 5° grid boxes by using an inverse-distance weighting method) and Reynolds SST (2003). The purple line indicates the regions in which the corresponding correlation is 95% statistically significant, assuming 1 degree of freedom per year ($r = \pm 0.27$). The box in the lower left indicates the TWP–N region.

periments, which may explain the weak SST variability simulated in the TWP (A02).

The statistical significance of the differences between ensemble means or subensemble means (tercile or quartile composites) is assessed via a Monte Carlo test (with replacement) for the observations and via a Student's *t* test for the model results. For information on the model's extratropical El Niño signal and a detailed diagnosis of the tropical atmospheric and oceanic changes during El Niño, the reader is referred to A02 and LN03, respectively.

3. Impact of the TWP on the observed extratropical response to El Niño in late fall

a. December to January changes in the extratropical sensitivity to tropical forcing

We begin by showing that the apparent change in the propagation path of the El Niño wave train from December to January does indeed reflect a spatial shift in the extratropical sensitivity to tropical forcing, from the west Pacific in late fall to the central Pacific in winter. Figure 2 shows observed SST and precipitation regressed against the North Pacific Index (NPI), which is a measure of the strength of the Aleutian low (Trenberth and Hurrell 1994). The regressions are computed separately for December and January for the period 1950–1999, and the sign convention is chosen so that warm SST and positive precipitation anomalies are as-

sociated with a deeper Aleutian low. The January regressions replicate the canonical ENSO signature, whereby interannual fluctuations in the strength of the Aleutian low are tied to SST and convection anomalies in the central/eastern tropical Pacific. In December, however, the sensitivity of the North Pacific circulation to tropical forcing east of the date line essentially vanishes: the SST regressions in that region are not even statistically significant, while the positive precipitation anomalies are confined to a small region south of the equator. Instead, there is now significant sensitivity to warm SST forcing in the TWP and to convective forcing in the northern TWP. The differences between the December and January NPI regressions are remarkable, considering that the SST and convective anomalies in the central/eastern Pacific during el Niño events are, if anything, stronger in December (Fig. 1), and they suggest that in late fall the El Niño wave train does not originate in the central tropical Pacific but in the TWP.

This spatial shift in the sensitivity of the North Pacific circulation, from the TWP in late fall to the central Pacific in winter, may be explained with simple Rossby waveguide arguments. Using influence functions, Newman and Sardeshmukh (1998) showed that the sensitivity of the North Pacific circulation to Rossby wave forcing over the TWP is greater in late fall (ND) than in winter (JF), whereas the opposite is true for forcing over the tropical central Pacific (their Fig. 3). They also showed that the sensitivity of the North Pacific circula-

tion to tropical divergence forcing in the eastern Pacific increases by roughly 50% from December to January, while that to western Pacific divergence forcing vanishes in January. Both changes appear consistent with the concomitant changes in the Pacific jet and associated Rossby waveguide. In January, when the jet is strongest, the waveguide is centered at 30°N all the way to the date line, but then it bends southeastward toward the westerly wind duct in the tropical eastern Pacific. Rossby waves generated in the TWP are steered by this waveguide and thus effectively become trapped within the tropics. In contrast, during late fall, the jet is weaker, but the waveguide extends zonally all the way across the North Pacific, so that Rossby waves emanating from the TWP can propagate into North America. This argument may explain why the North Pacific circulation only feels the forcing from the TWP in late fall. The increased January sensitivity to eastern Pacific forcing, on the other hand, may also be due to the stronger jet, which results in a stronger vorticity gradient and a stronger subtropical Rossby wave source for a given amount of divergence (note that waves generated in the tropical eastern Pacific are going *across* the waveguide, unlike waves originating in the TWP, which are more channeled within it).

b. Impact of the TWP on the extratropical response to El Niño in late fall

The above results suggest that the observed El Niño extratropical response during late fall is strongly influenced by SST and convection anomalies in the TWP. To explore this possibility, and guided by the December SST regression (Fig. 2), we constructed a simple index of SST in the northern tropical west Pacific region (TWP–N) by averaging detrended monthly mean SST anomalies over the box (3°–15°N, 135°–155°E; see Fig. 2) for the period 1950–99. We then stratified El Niño events by their December TWP–N SST index value (Fig. 3a). The nine events chosen (also shown in Fig. 3a) are the same as those used for the composites in Fig. 1 and identified by Trenberth (1997), to which we have added the 1997/98 event (as in A02). Based on this December TWP–N SST index, the three events in the HIGH and LOW terciles of El Niño anomalies occur in 1969, 1987, and 1997 and 1965, 1972, and 1991, respectively.[3]

Figure 4 shows difference maps of December HIGH−LOW tercile composites of 200-hPa height

(Z_{200}), precipitation, SST and surface zonal wind; these anomalies should be viewed as relative to the mean El Niño pattern, not climatology.[4] The HIGH−LOW SST pattern has widespread warm anomalies in the TWP (particularly north of the equator) that are accompanied by warmer SST anomalies in the far eastern tropical Pacific and cold SST anomalies in the central tropical Pacific. The differences between the HIGH/LOW composites themselves can best be described as an absence of the cold SST "horseshoe" pattern—including the cooling in the TWP—in the HIGH composite, as well as an eastward shift in the location of the warmest SST anomalies from the central to the far eastern tropical Pacific (not shown). The corresponding HIGH−LOW precipitation anomalies (Fig. 4b) are somewhat noisy but indicate enhanced convection in the TWP (also evident using NCEP reanalysis precipitation rate data, not shown). The HIGH−LOW Z_{200} pattern (Fig. 4a) is consistent with the regression results (Fig. 2) and confirms that an enhanced extratropical response to El Niño occurs in December when warm SST conditions and enhanced convection prevail in the TWP (in contrast, the LOW composite exhibits a ridge in the North Pacific; not shown). Moreover, the HIGH−LOW surface zonal wind pattern (Fig. 4d) suggests a weakened tropical bridge from the eastern to the western Pacific, with near-normal (enhanced) trade winds in the far TWP in the HIGH (LOW) composite (not shown). The corresponding 500-hPa vertical velocity composites also illustrate this weakened and eastward-shifted Walker cell, with anomalous equatorial upward motion at 160°E (not shown).

The above results thus suggest that the late fall differences in both the TWP and the extratropics between HIGH and LOW El Niño events are due to differences in the anomalous Walker cell, which in turn may be related to differences in the details of El Niño warming in the eastern tropical Pacific. That is, certain "flavors" of El Niño, characterized by a reduced and eastward-shifted west–east SST gradient near the date line, may produce a weaker bridge to the TWP. Whereas for a "typical" El Niño, enhanced trade winds cool the TWP, for the "weak bridge" events, the trades do not strengthen, allowing relatively warm SST conditions to persist in the TWP. These warm SSTs favor the development of convection and, because of the enhanced sensitivity of the North Pacific circulation to TWP forcing in late fall, result in a stronger El Niño teleconnection.

---

[3] The selected HIGH and LOW years (i.e., Fig. 3) are not changed if this SST index is not detrended or if the size of the box used to define the TWP–N index is made larger or smaller.

[4] That is, to approximately recover the HIGH (LOW) El Niño Z_{200} December composite, one needs to add (subtract) the pattern in Fig. 4a (with the amplitude halved) to that in Fig. 1a, ignoring the (small) nonlinearity in the response.
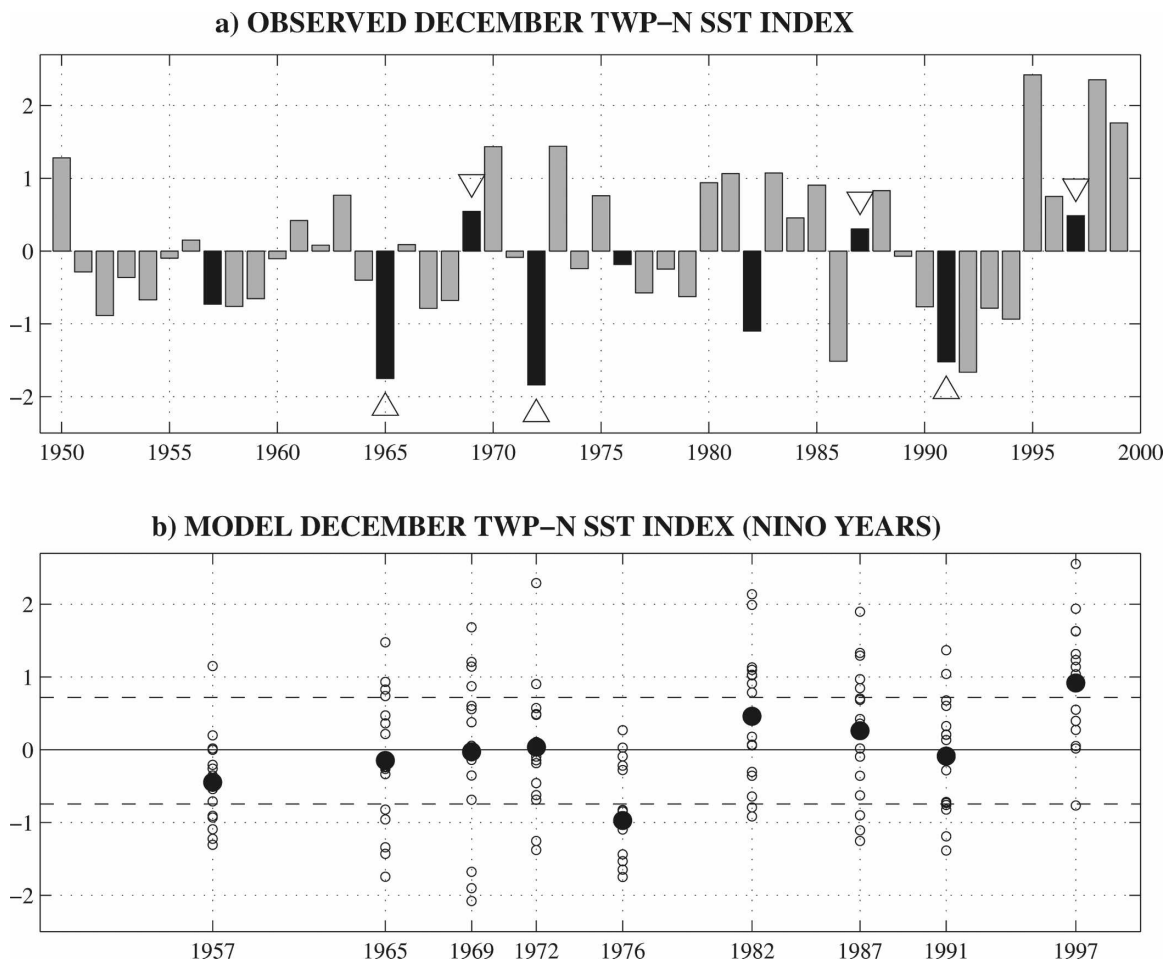
a) OBSERVED DECEMBER TWP–N SST INDEX

b) MODEL DECEMBER TWP–N SST INDEX (NINO YEARS)

FIG. 3. (a) Observed December TWP–N SST index for the period 1950–99. The index is defined as the detrended standardized SST averaged over the region (3°–15°N, 135°–155°E). The nine El Niño years are indicated with black bars. The three LOW and HIGH El Niño years, as defined by this TWP–N SST index, are indicated by triangles and inverted triangles, respectively. See Figs. 2 or 4c for the location of the TWP–N box. (b) Simulated December TWP–N SST index for the nine El Niño years and for each realization in the MLM experiment. The circles denote individual realizations; the black dots denote the ensemble average for each El Niño event. The dashed lines denote the 25% and 75% percentiles and indicate which realizations enter the UPPER and LOWER quartile composites in the left of Fig. 7.

While the observational results are consistent with the above hypothesis, they are far from conclusive. In addition to the very small sample size, we cannot distinguish between TWP SST anomalies driven by details of El Niño and its tropical bridge from those that are generated by other (oceanic) processes. Moreover, even if we had enough data to unambiguously relate the TWP SST anomalies to El Niño differences, it would not necessarily mean that those TWP SSTs force the extratropical response, since the altered tropical bridge could be directly inducing the anomalous TWP convection (through the same changes in surface winds and convergence that give rise to the TWP warming). That is, the changes in TWP SST would be a *by-product* of the perturbed bridge, and the extratropical circula-

tion anomalies would be directly forced by central tropical Pacific SSTs (so that a coupled model would not be needed to simulate this effect). To address some of these issues, we now examine the results of a similar analysis performed on the MLM model runs.

4. Impact of the TWP on the fall extratropical response to El Niño in model simulations

Recall that in the MLM runs, SST variability in the TWP can arise as a result of forcing by local weather noise or as a response to an atmospheric bridge (ENSO induced or otherwise), not from oceanic advection—although air–sea feedbacks may modify the SST response. Additionally, each MLM ensemble member
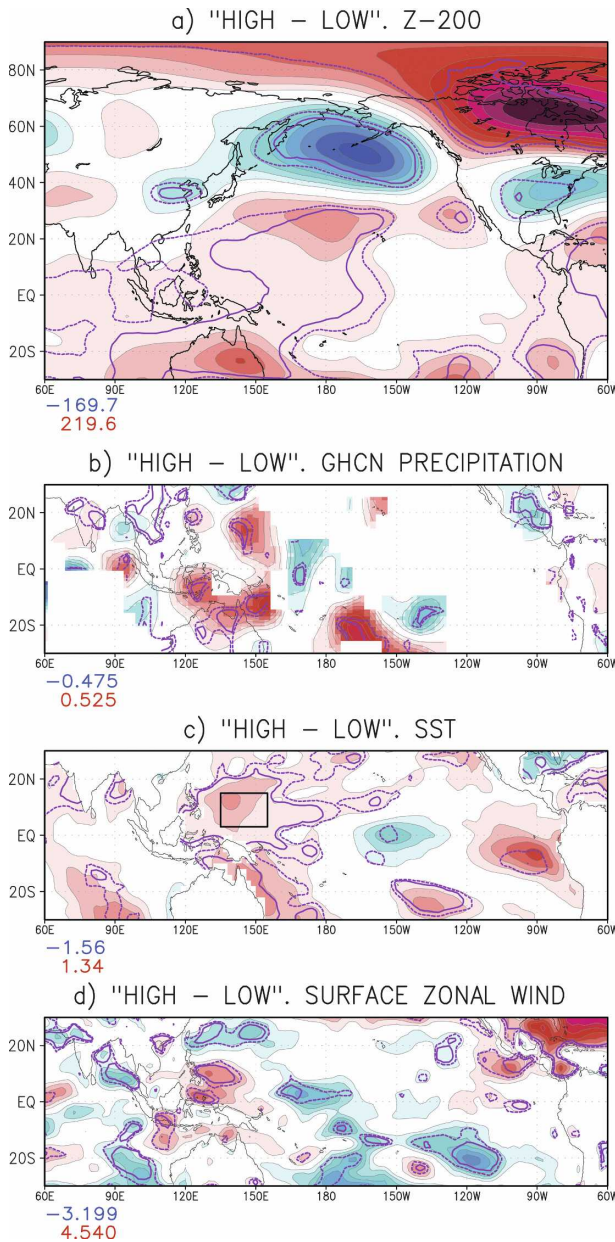
a) "HIGH − LOW". Z−200

b) "HIGH − LOW". GHCN PRECIPITATION

c) "HIGH − LOW". SST

d) "HIGH − LOW". SURFACE ZONAL WIND

FIG. 4. Observed El Niño December anomalies stratified according to the December TWP–N SST index shown in Fig. 3a, so as to produce "HIGH and LOW" tercile composites. Upper tercile years are 1969, 1987, and 1997; lower tercile years are 1965, 1972, and 1991 (see Fig. 3a). The area used to define the TWP−N SST index is indicated by the box in (c). Shown are HIGH−LOW tercile composite patterns of (a) 200-hPa geopotential height, (b) tropical precipitation, (c) tropical SST, and (d) tropical surface zonal wind. Contour/shading interval is 20 m for height, 0.067 cm day^{-1} (20 cm month^{-1}) for precipitation, 0.25 K for SST, and 0.5 m s^{-1} for winds. Red (blue) shadings indicate positive (negative) values. The zero contour is omitted and shading starts at the lowest contour. The dotted (solid) purple line indicates statistical significance of the HIGH−LOW composite differences at the a posteriori (two-sided) 80% and 90% confidence levels. Note that wherever the sign of the difference is expected a priori (i.e., enhanced TWP−N convection, negative North Pacific heights), the significance levels are actually 90% and 95%.

produces different SST anomalies for a given month (outside of the specified region), so that each El Niño event in each ensemble member can be considered an independent realization ($16 \times 9 = 144$ samples in total).

We begin by comparing the overall sensitivity of the North Pacific circulation to tropical forcing in December and January (Fig. 5, the model counterpart to Fig. 2). Clearly, the model does not reproduce the dramatic spatial/temporal shift in sensitivity seen in the observations, particularly for the SST field (note that the lack of GHCN data in the eastern Pacific exacerbates the model-to-observation precipitation differences in that region). In qualitative agreement with the observations, however, the largest positive precipitation regressions are found in the TWP in December but in the central Pacific in January. The observed NW–SE-oriented dipolar structure of the December TWP precipitation anomalies is also well reproduced, with positive (negative) anomalies north (south) of Indonesia (cf. Figs. 2a, 5a).

The model's inability to simulate but a modest shift in the extratropical sensitivity of the North Pacific circulation to tropical forcing may be related to the fact that in January, the Pacific jet is weaker and farther poleward than observed (Alexander and Scott 1995), which results in small fall-to-winter changes in the Rossby waveguide (Newman and Sardeshmukh 1998). Another source of error is the model's underestimation of SST variability in the TWP (A02). One consequence of these deficiencies is that the simulated composite El Niño extratropical response is similar in December and January (not shown, but see Fig. 12 in A02).

Nevertheless, this El Niño response does exhibit enhanced sensitivity to TWP forcing, relative to central Pacific forcing, in December compared to January. This can be seen by computing corresponding regressions using El Niño years only (Fig. 6), where again the regressed patterns should be viewed as relative to the mean El Niño pattern (note that this calculation cannot be done with observed data because there are only nine El Niño samples). The presence of convection and warm SST anomalies in the TWP in December (together with enhanced warming in the far eastern Pacific) is clearly associated with a stronger El Niño response (deeper Aleutian low), unlike in January when the modulation of the El Niño response is mostly due to *central* tropical Pacific SST/convection anomalies. Thus, while this model cannot be used to diagnose the differences between the December and January El Niño teleconnection, this result gives us some confidence in the model's usefulness for studying the linkages between the El Nino teleconnection and the TWP in late fall.
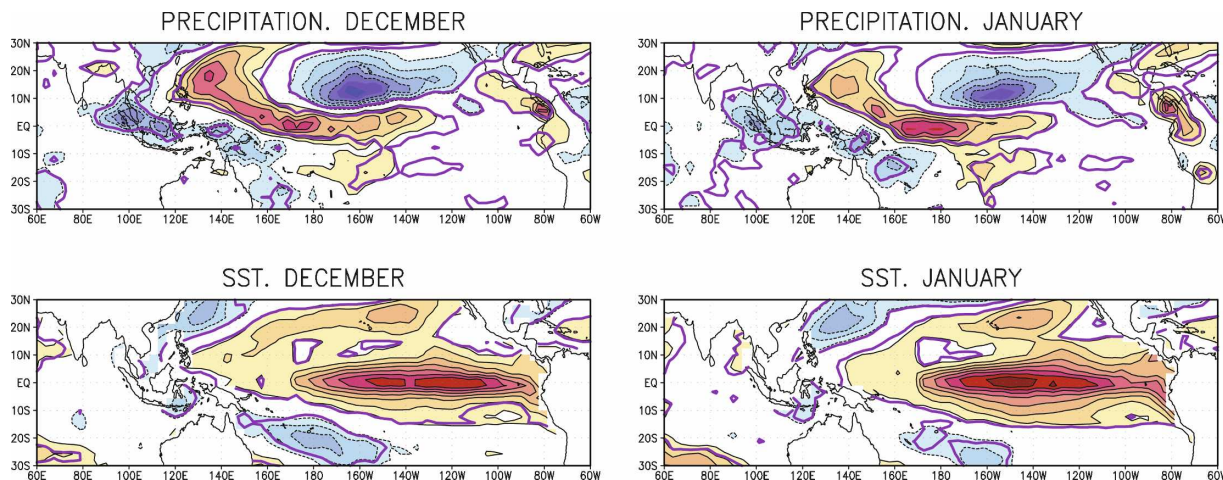
FIG. 5. Same as Fig. 2, but for the MLM experiment (every model realization is considered an independent realization, i.e., the sampling size is 800). The model's NPI std dev is 4.1 hPa in December and 4.6 hPa in January. Contour interval as in Fig. 2. The purple line indicates the regions in which the corresponding correlation is 99% statistically significant, assuming 1 degree of freedom per year ($r = \pm 0.09$).

The simulated December TWP–N SST index for each ensemble member during each El Niño event is shown in Fig. 3b (note that the intraevent variability exceeds the interevent variability). Using this index, we now stratify our 144-member sample of December El Niño responses to produce upper and lower quartile composites (Fig. 7, left, to be compared with the observational tercile composites in Fig. 4). The UPPER− LOWER Z_{200} pattern (Fig. 7a) indicates an enhanced El Niño wave train when the TWP is warmer than normal (Fig. 7c). As in the observed HIGH−LOW tercile composite, there is also enhanced warming in the far eastern Pacific, that is, an increased west–east SST gradient (although the central Pacific is slightly warm rather than cool). Other aspects of the observed com-

posite that are mimicked in the simulation include the northeastward extension of the TWP SST anomalies into the subtropics and the anomalous westerly winds in the TWP (Fig. 7d). The latter is consistent with our hypothesis that the warming in the TWP occurs as a result of a weakened tropical bridge. The precipitation pattern, however, exhibits only weak anomalies in the TWP and stronger anomalies in the central tropical Pacific, so it is not clear which anomaly makes a greater contribution to the extratropical response (note that the corresponding regression pattern, Fig. 6a, displays comparable anomalies in both regions).

In addition, the model TWP–N SST index exhibits substantial random variability within each El Niño event (Fig. 3b). There does appear to be a deterministic
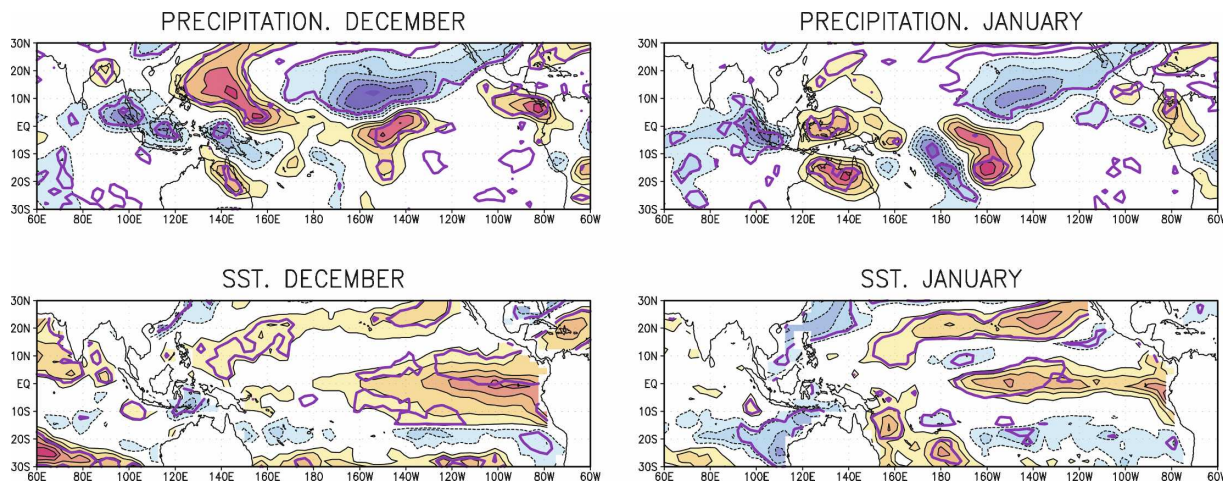

FIG. 6. Same as Fig. 5, but for El Niño years only (i.e., the sampling size is 144). Contour interval as in Fig. 5. The purple line indicates the regions in which the corresponding correlation is 95% statistically significant, assuming 1 degree of freedom per year ($r = \pm 0.16$).
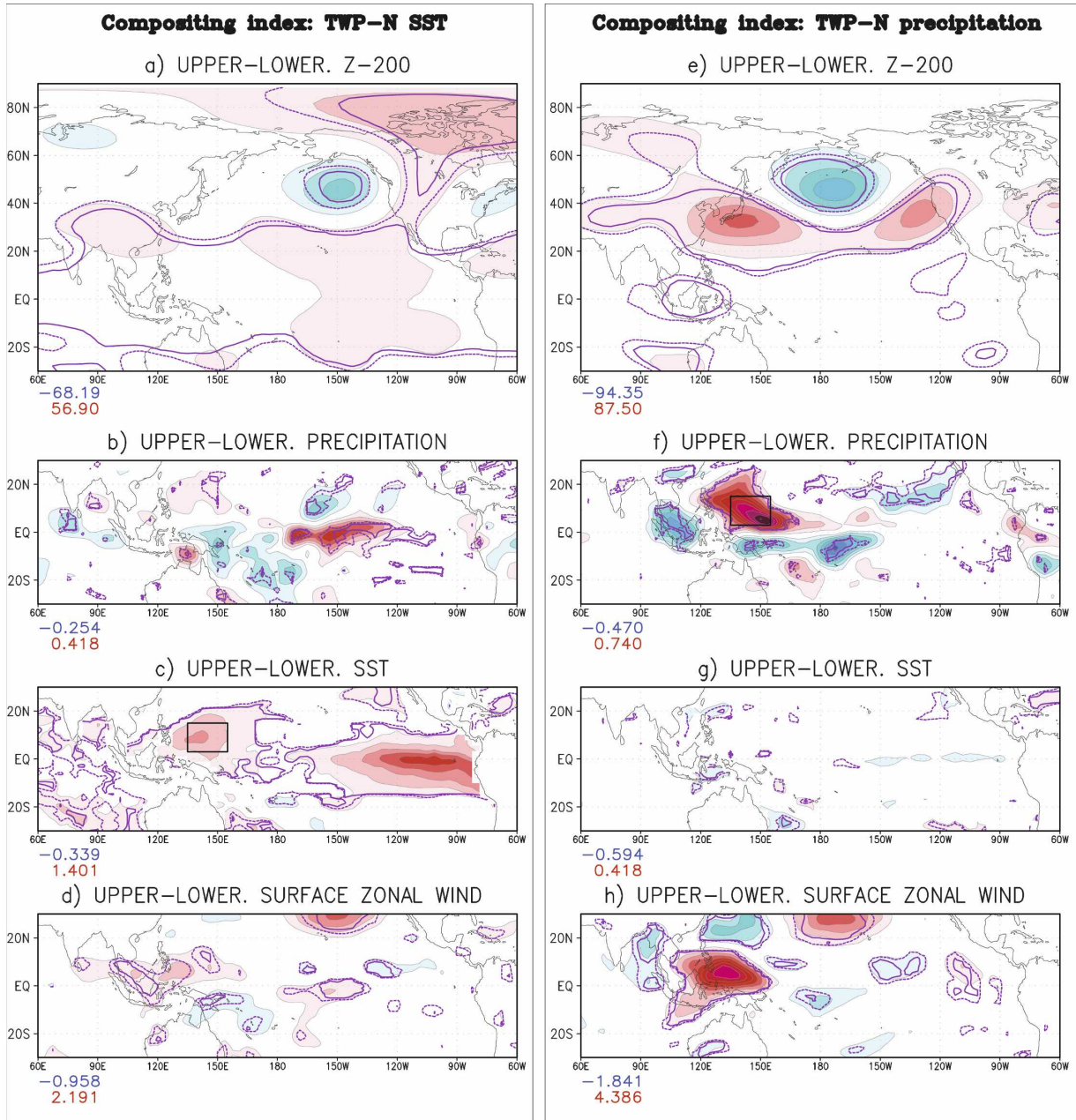
FIG. 7. (left) Similar to Fig. 4, but for the MLM experiment. Simulated El Niño December anomalies stratified according to the December TWP–N SST index shown in Fig. 3b, so as to produce UPPER and LOWER quartile composites (each containing 36 samples). (c) The area used to define the TWP–N index is indicated by the box. Contour/shading interval is the same as in Fig. 4 (20 m for height, 0.067 cm day^{-1} for precipitation, 0.25 K for SST, and 0.5 m s^{-1} for wind). The zero contour is omitted and shading starts at the lowest contour. The dotted (solid) purple line indicates statistical significance of the UPPER−LOWER composite differences at the a posteriori (two-sided) 95% and 99% confidence levels. Note that wherever the sign of the difference is expected a priori (i.e., enhanced TWP–N convection, negative North Pacific heights), the significance levels are actually 97.5% and 99.5%. (right) Same as left, but composites are based on the TWP–N precipitation index (box in panel f).

component to this variability inasmuch as some events clearly have warm (1997) or cold (1976) ensemble-mean TWP−N SST values, but the ensemble-mean tercile distribution of the simulated index does not exhibit

a good correspondence with the observed one (there are only two HIGH/warm and one LOW/cold event in common). These results suggest that the deterministic signal is small compared to the random component

driven by atmospheric noise and/or is not well simulated by the model. Thus, the model provides only limited support for the hypothesis that the TWP SST anomalies (and their effect on the extratropical El Niño response) are partly driven by specific details of the El Niño SST forcing in the central/eastern tropical Pacific.

Nevertheless, the model is still useful for studying the fall sensitivity to forcing from the TWP. For instance, another source of noise that could force an extratropical response is intrinsic TWP convection variability *not* induced by local SST anomalies. As could be expected from Fig. 6, a much stronger extratropical height signal can be found in UPPER−LOWER quartile composites based on an index of precipitation in the TWP–N region (Fig. 7, right). The resulting precipitation pattern (Fig. 7f) is similar to the corresponding composites based on TWP–N SST (Fig. 7b), but the TWP convective anomalies are much stronger and more widespread, with a well-defined NW–SE dipolar structure. In contrast, there is no signal in the SST field (Fig. 7g). Both this result and the regressions in Fig. 6 suggest that in December, the North Pacific El Niño teleconnection is particularly sensitive to this dipole pattern of TWP precipitation, which can occur as a result of natural tropical atmospheric variability (i.e., atmospheric noise) but may also be excited by SST anomalies in the TWP. Indeed, for the 1997 "warm TWP" El Niño event, both the ensemble-mean TWP precipitation and Z_{200} height anomalies are significantly stronger in December in the coupled MLM experiment than in the uncoupled one (not shown), supporting the premise that coupling-induced warming in the TWP can drive convection aloft and thereby enhance the extratropical December El Niño teleconnection.

Although, for the sake of simplicity, we have used the same box to construct the TWP−N SST and precipitation indices, in reality the precipitation response may not be exactly collocated with the SST forcing. In addition, the full effect of coupling may not just entail changes in the mean SST/convection in the TWP but may also involve changes in the convection distribution (see section 5).

5. Impact of the TWP on the late fall extratropical response to the 1997/98 El Niño

Drawing rigorous conclusions from the model study of the previous section is made difficult by the conflation of differences among El Niño events (some of which did not produce mean warming in the TWP; Fig. 3b) and noise in the simulations. To clarify these issues, we next describe the results of a very large ensemble of simulations of a single E1 Niño event (1997/98), for

which warm TWP conditions occurred both in nature and in the model (Figs. 3a,b). Analyzing a single event allows for a much cleaner assessment of the deterministic impact of TWP coupling, which is now driven by specific details of that El Niño event, as opposed to many different events. The large ensemble also facilitates the separation of the mean signal driven by mean warm SSTs in the TWP from the variance (noise) forced by variability in TWP precipitation. To reduce other sources of noise and focus on the effects of the TWP, coupling in this TROPMLM experiment is confined to the tropics of the western hemisphere (TWP and Indian Ocean, recall section 2).[5]

We begin by examining the changes in the extratropical December El Niño response due to coupling-induced mean warm conditions in the TWP (Fig. 8). In this simulation, the mean warming in the TWP for this event is not maximized in the TWP–N box but is centered on the equator (Fig. 8e) and is a residual from the previous month (not shown; note that the bull's-eye-like extension of the warm equatorial tongue is an artifact of the sharp boundary at 172°E between prescribed and predicted SSTs). The main effect of this coupling-induced warming on the tropical precipitation field is to enhance precipitation aloft, including part of the TWP–N region (Fig. 8d), which acts to reduce the negative precipitation El Niño anomaly (west of the date line, Fig. 8c). This enhanced convection over warmer waters can simply be attributed to increased evaporation and hydrostatic reduction of surface pressure due to low-level warming (Fig. 8f; Lindzen and Nigam 1987). Although the positive SST and precipitation anomalies are somewhat offset relative to the TWP–N box, the extratropical El Niño response is once again stronger in the coupled experiment, with a 20% enhancement in the strength of the Z_{200} North Pacific anomaly (Figs. 8a,b), and greater differences at lower levels (25%, 30%, and 35% at 500 and 850 hPa and at sea level, respectively; not shown). This result replicates our earlier finding for the MLM experiment, but the effect is now more readily attributable to the warm TWP SST anomalies (Fig. 8e). Thus, coupling-induced warming in the TWP indeed promotes enhanced convection aloft and a stronger El Niño response. Although we have not attempted to diagnose this oceanic warming, lacking a one-way coupled simulation that would isolate the atmospheric forcing, it is conceivable that this warming could originally be due to reduced

---

[5] Because the SST anomalies in the Indian Ocean are very small (see Fig. 8e), our assumption throughout this paper that the impact of coupling on TWP convection is due to *local* coupling is justified.
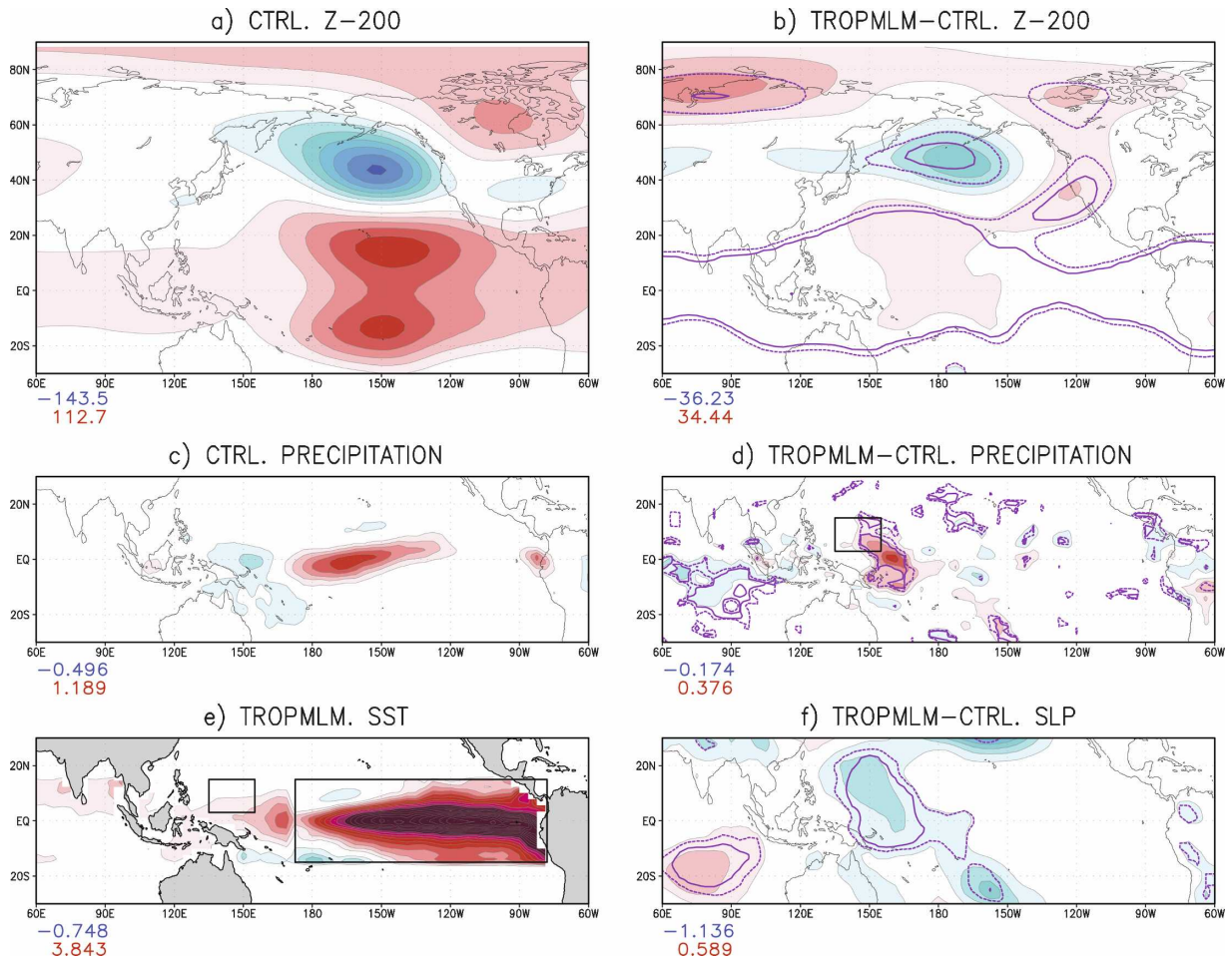
FIG. 8. December 1997 ensemble-mean anomalies of (a) uncoupled (CTRL) 200-hPa height, (c) CTRL precipitation, and (e) TROPMLM (entire domain) and CTRL (eastern Pacific box only) SST. Coupled minus uncoupled ensemble-mean anomalies of (b) 200 hPa height, (d) precipitation, and (f) SLP. Contour interval is 20 m, 10 m, 0.2 cm day^{-1}, 0.067 cm day^{-1}, 0.2 K, and 0.2 hPa, respectively. The zero contour is omitted. The dotted and solid purple lines denote statistical significance of the coupled–uncoupled differences at the a posteriori (two sided) 95% and 99% confidence levels. The specified SST region in the tropical eastern Pacific (large rectangular box) and the TWP–N box are indicated in (e) for reference.

trade winds, following which the ocean transfers the heat back to the atmosphere.

We are also interested in confirming the sensitivity of the extratropical El Niño response to TWP–N convection for fixed SST conditions in the eastern tropical Pacific (i.e., in the absence of contaminating sources of variability from this region). For this purpose we again stratified the TROPMLM ensemble using the TWP–N precipitation index. The corresponding UPPER−LOWER quartile composites of Z_{200} and precipitation (Figs. 9a,b) are very similar to those obtained for the MLM experiment (Figs. 7e–f): they reveal a very pronounced and significant wave train propagating from the TWP–N region toward the North Pacific and North America and emanating from a broad band of convective anomalies that stretches northwestward from the

equatorial date line to the Philippines, with weaker negative anomalies to the southwest. Moreover, an "extratropical wave train" index defined as the difference between the (area averaged) height anomalies in the northern Pacific and western Pacific centers of action (Fig. 9a) is correlated with the TWP–N precipitation index at 0.45 (Fig. 10). These results confirm that tropical precipitation anomalies in the TWP (which may arise irrespective of any SST forcing, but may also be generated by coupling in the TWP) excite a wave train that interferes constructively with the main El Niño wave train emanating from the central equatorial Pacific (Fig. 8a). The result is an enhanced (damped) El Niño teleconnection in the presence (absence) of convection in the TWP (Fig. 9c). Moreover, in the presence of TWP convection, the December El Niño wave train
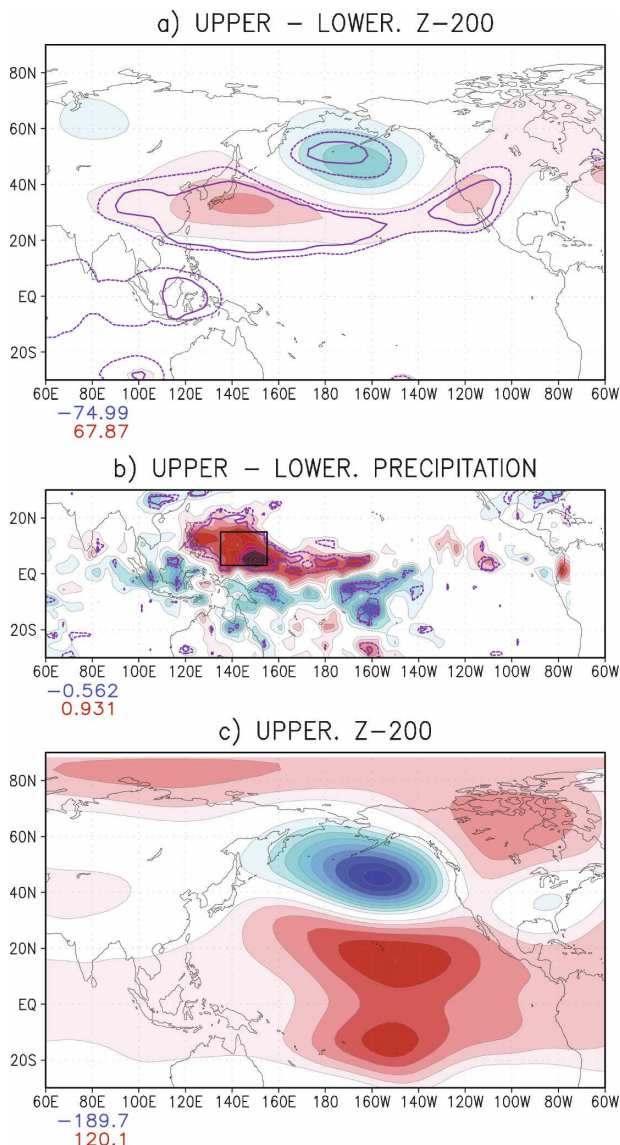
a) UPPER − LOWER. Z−200

−74.99
67.87

b) UPPER − LOWER. PRECIPITATION

−0.562
0.931

c) UPPER. Z−200

−189.7
120.1

FIG. 9. UPPER−LOWER quartile composite differences, based on the TWP–N precipitation index, of (a) 200-hPa height and (b) precipitation anomalies for December 1997 in the TROPMLM experiment. Contour/shading interval is 20 m and 0.0667 cm day^{-1}, respectively. Red (blue) shadings indicate positive (negative) values. The zero contour is omitted and shading starts at the lowest contour. The dotted (solid) purple lines indicate statistical significance of the UPPER−LOWER differences (95% and 99% two-sided confidence levels). The sample size in each UPPER/LOWER composite is 25. (bottom) Also shown is the UPPER quartile composite of 200-hPa height [same contour interval as in (a)].

features positive height anomalies over the subtropical western North Pacific (Fig. 9c), reminiscent of the corresponding observed El Niño wave train for mean and anomalously warm TWP conditions (Figs. 1a, 4a).

We still need to address the following questions:

Does coupling change the distribution of TWP–N convection and does coupling also change the extratropical sensitivity to this forcing? The impact of coupling on both the mean and the variance of TWP–N convection can be seen in Fig. 11, a comparison of histograms of the TWP–N precipitation index in the TROPMLM and CTRL experiments for December 1997 and January 1998. Because of the large sampling size, these histograms can be used to estimate the probability distribution functions (PDF) of the TWP–N index. Clearly, the coupling-induced changes in December are not linear: the TROPMLM PDF is not merely shifted toward heavier mean precipitation relative to CTRL but has increased variance and is more strongly skewed toward positive values. This coupling-induced shift in the December TWP–N precipitation PDF then impacts the extratropics enhancing the El Niño response, as illustrated in Fig. 8b and also seen in the scatterplot of the TWP–N precipitation index against the extratropical wave train index (see thick dot and cross marks in Fig. 10). Note that there is substantial overlap of the clouds of points from the TROPMLM and CTRL experiments and both exhibit the same correlation between the precipitation and wave train indices (−0.5). This result suggests that the linkage between the TWP–N convection and the extratropical response does not depend on coupling. To first order, then, the effect of coupling is simply to shift the distribution of TWP–N convection toward higher values, which results in a shift of the Z_{200} distribution toward higher (negative) values and hence a stronger ensemble-mean El Niño response. The concurrent increase in TWP–N convection variance (which does not increase the variance of the extratropical signal; not shown) may also play a role in modifying the extratropical response.

Finally, one reason we focused on the December response to the 1997/98 El Niño is that in January, coupling in the TWP has virtually no effect on convection (Figs. 11c,d). This may be due to a number of factors. First, in January, the mean SST in the TWP is between 0.5° and 1°C cooler (not shown). More important, the main area of ENSO-induced convection in the central equatorial Pacific is displaced southward and precipitation in the TWP is strongly suppressed (not shown). Both the presence of mean subsidence and cooler SST conditions may explain why, in midwinter, coupling impacts neither the convection in the TWP–N region nor the El Niño teleconnection.

6. Summary and concluding remarks

The observational results presented in this study indicate that there is a dramatic seasonal and spatial shift
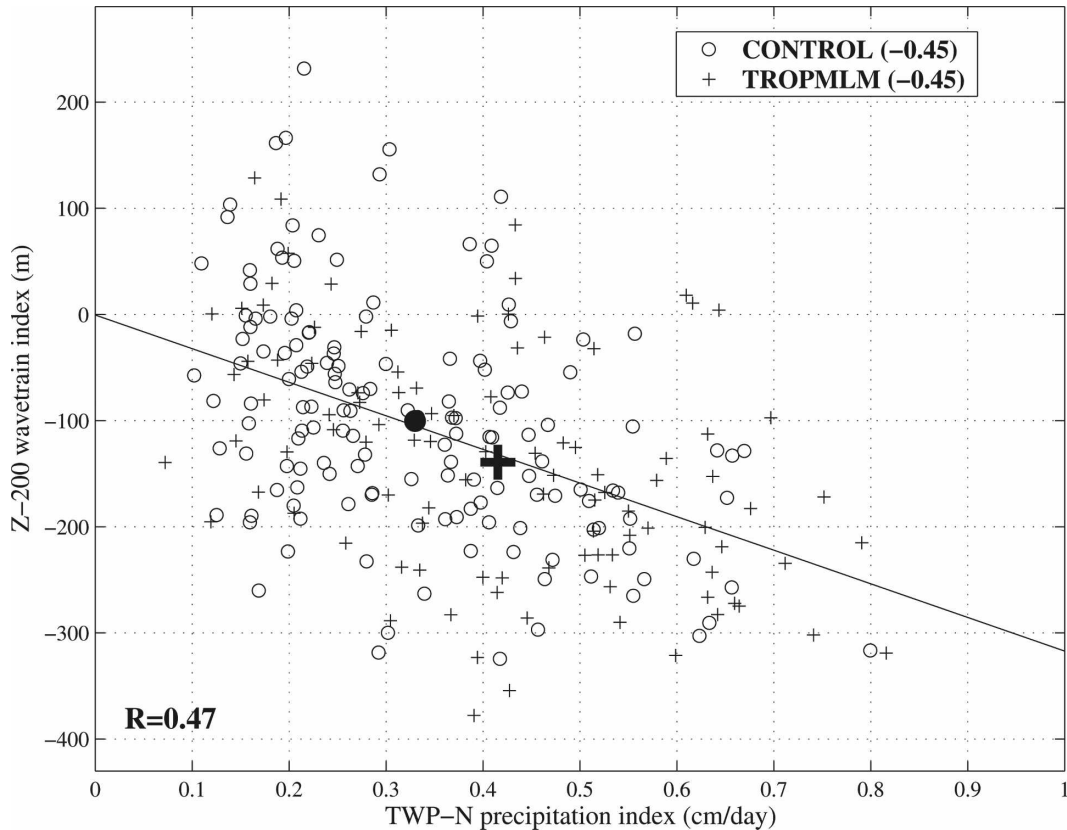
FIG. 10. Scatterplot between the December 1997 TWP–N precipitation index and the 200-hPa North Pacific wave train index in experiments CTRL and TROPMLM. The precipitation index is defined as the total precipitation averaged in the TWP–N region. The 200-hPa North Pacific wave train index is defined as the difference between the 200-hPa anomalies averaged over the northern Pacific and western Pacific centers of action in Fig. 9a (areas within the ±60-m contour). The number in the bottom left corner indicates the correlation coefficient obtained pooling all data together. The correlation for each individual experiment is indicated in the legend box. The solid line represents a linear fit to the data. The thick dot and cross represent the ensemble-mean CTRL and TROPMLM values, respectively.

in the sensitivity of the North Pacific/North American circulation, from the tropical western Pacific (TWP) in late fall to the tropical central/eastern Pacific (TEP) in winter. This sensitivity shift, which is consistent with the attendant changes in the basic-state jet and associated Rossby waveguide (Newman and Sardeshmukh 1998), implies that SST and/or convective anomalies in the TWP can potentially play a prominent role in forcing extratropical flow anomalies in late fall. In particular, the El Niño teleconnection at this time of year appears to be determined to a large extent by forcing in the TWP, being substantially stronger when warm conditions and convection prevail in the northern TWP.

In light of our results, we propose the following hypothesis for El Niño teleconnection. In winter, the tropical bridge and the interannual SST seesaw between the TWP and the TEP (Chen 2002) are usually well established for both weak and strong El Niño

events. Additionally, the North Pacific circulation is more sensitive to forcing from the TEP, so the El Niño teleconnection depends mainly on this TEP forcing. In late fall, however, some El Niño events characterized by a reduced and/or eastward-shifted west–east SST gradient east of the date line also feature a weakened tropical bridge to the TWP (i.e., reduced subsidence and near-normal trade winds), allowing warm oceanic conditions in the TWP that are conducive to the development of local convection (in contrast to the cold SSTs/suppressed convection that occur when the bridge is strong). Because of the enhanced sensitivity of the North Pacific circulation to forcing from the TWP in late fall, the extratropical El Niño response will be strong. The most recent 2006/07 El Niño event, which decayed rapidly in January but was strong in December, appears to agree with this picture, with maximum warming displaced toward the far TEP, warm SSTs and

a) DECEMBER 1997. CTRL

mean = 0.32
std = 0.14

b) DECEMBER 1997. TROPMLM

mean = 0.42
std = 0.18

c) JANUARY 1998. CTRL

mean = 0.23
std = 0.14

precipitation (cm/day)

d) JANUARY 1998. TROPMLM
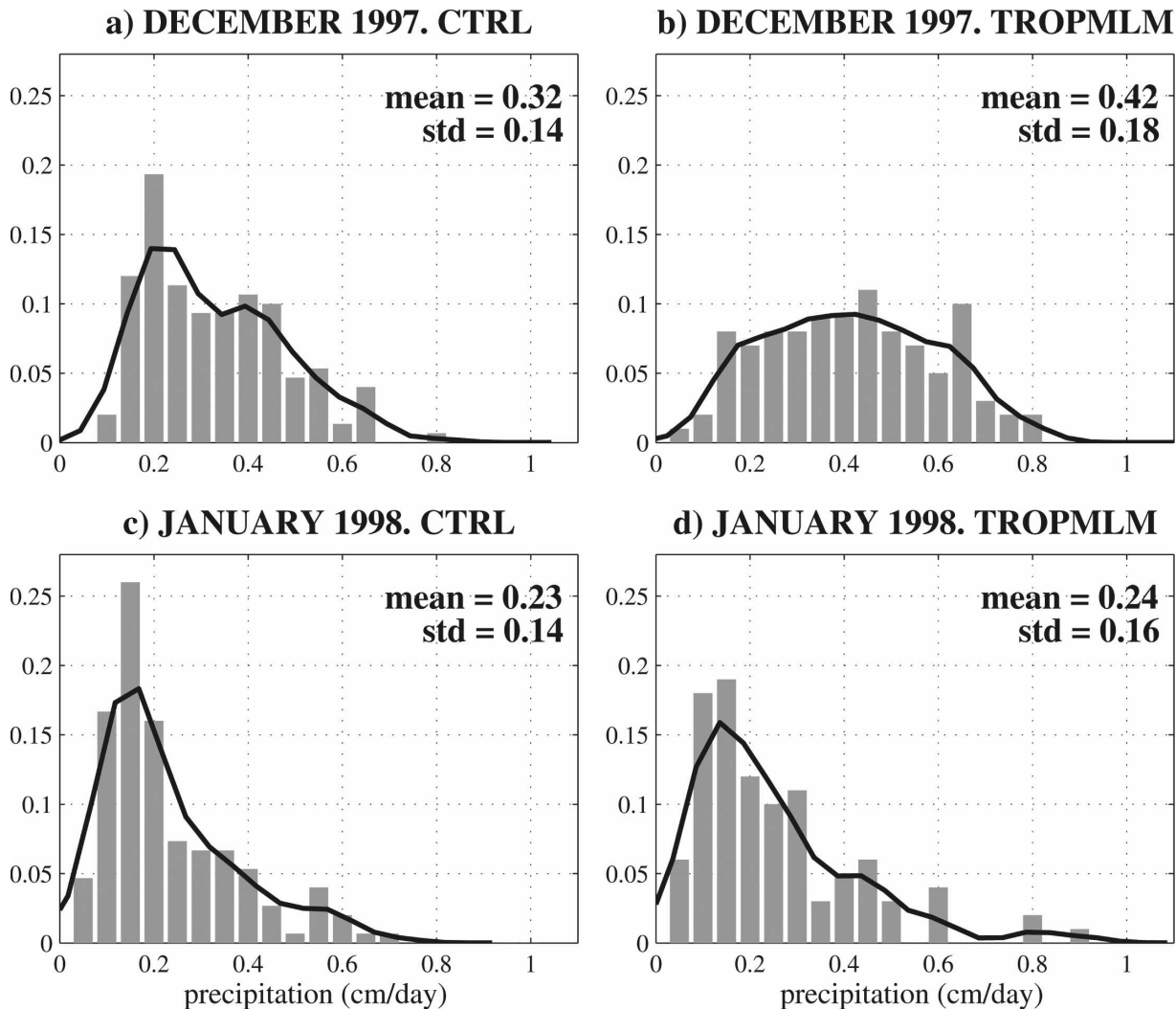
mean = 0.24
std = 0.16

precipitation (cm/day)

FIG. 11. Normalized histogram (bars) and probability density function (lines), estimated with a Gaussian Kernel, of monthly mean (top) December 1997 and (bottom) January 1998 total precipitation (in cm day-1) averaged over the TWP–N region, in the (left) 150 CTRL and (right) 100 TROPMLM simulations.

convective anomalies in the TWP, and a pronounced extratropical wave train response in late fall (Fig. 12).

Although the GFDL model substantially underestimates the overall observed seasonal shift in the sensitivity of the North Pacific circulation, it does produce an El Niño response that is itself much more sensitive to TWP forcing, particularly convective forcing, than to TEP forcing in late fall. An enhanced El Niño teleconnection then occurs when anomalous convection, either "natural" or forced by warm SSTs, occurs over the TWP (though, again, the sensitivity to SST forcing is rather weak). Furthermore, a very large ensemble simulation of the single 1997/98 El Niño event allowed for unambiguous identification of the deterministic impact of coupling-induced warming in the TWP on the

extratropical El Niño response. This experiment revealed a clear enhancement of the coupled El Niño teleconnection during late fall as a result of warming in the TWP, which in turn favored the development of convection in the northern TWP.

Taken together, our model results provide partial support for the view that the late fall SST differences in the TWP from event to event—and their impact on the extratropical El Niño response—may be partly deterministic and driven by details of the El Niño SST anomalies in the TEP, via changes in the tropical atmospheric bridge. Of course, this deterministic effect may be obscured by other sources of TWP SST variability. In our regionally coupled experiments, random SST variability driven by atmospheric noise clearly had an
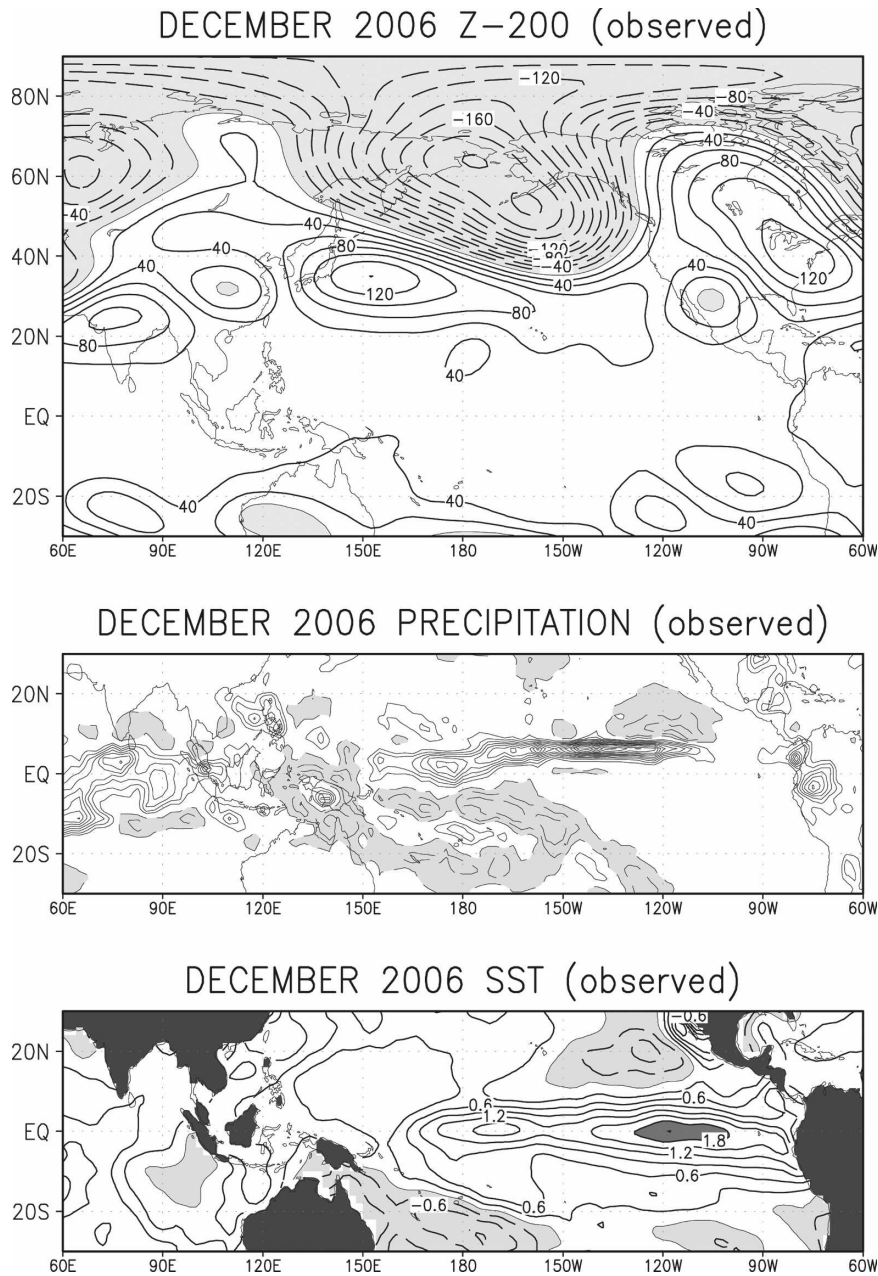
DECEMBER 2006 Z-200 (observed)

DECEMBER 2006 PRECIPITATION (observed)

DECEMBER 2006 SST (observed)

FIG. 12. Observed NCEP Z_{200}, GPCP precipitation, and NOAA SST December anomalies for the 2006/07 El Niño event. The anomalies are computed relative to the 1950–99 climatology (for consistency with the rest of the paper), except for the GPCP data (for which the climatology can only be computed for the period 1979–99). Contour/shading interval is 20 m, 0.15 cm day^{-1} and 0.3 K, respectively. The zero contour is omitted and shading starts at the lowest contour (except in the lower panel). Negative contours are lightly shaded.

influence on whether the TWP was warm during a particular realization of a given El Niño event. Moreover, in nature, SST variability in the TWP can also result from random oceanic processes or long-term variability unrelated to El Niño.

The inability of the GFDL model to reproduce but a modest seasonal shift in the sensitivity of the North Pacific circulation to tropical forcing is tied to deficiencies in the simulated basic-state winds and may be endemic to all GCMs. This is a topic of current research,

as is diagnosing the December and January differences in the El Niño teleconnection, with either a simpler model or a GCM that better reproduces the observed differences in the fall/winter El Niño signal.

Our results serve to reiterate the point (perhaps often overlooked, although undoubtedly familiar to seasonal forecasters/analysts) that the "canonical" view of the El Niño teleconnection—a TNH-like wave train emanating from the central/eastern equatorial Pacific—is more appropriate in midwinter than in late fall (e.g., Wang and Fu 2000). Diagnostic studies using DJF seasonal averages may therefore obscure some important aspects of climate anomalies associated with El Niño.

While our focus has been on El Niño, the results are also relevant for La Niña and non-ENSO situations characterized by convective forcing in the TWP, such as occur, for instance, during the passage of MJO disturbances. For example, the presence of warm SST anomalies and convection in the TWP in December during the La Niña 2005/06 event may explain why the circulation responded with a pronounced North Pacific jet more characteristic of El Niño conditions, even though the SST and convective anomalies in the TEP were typical of a La Niña (K. Weickmann 2006, personal communication). Several previous studies have demonstrated a relationship between SST and/or convective forcing in the TWP and atmospheric circulation anomalies over the North Pacific/North America in winter, both during El Niño (Hamilton 1988; Chen 2002) and in general (Simmons et al. 1983; Palmer and Owen 1986; Quan et al. 2006). Yet, our results suggest that they may have mixed together late fall and winter effects. Additionally, Quan et al.'s (2006) identification of the (subtropical) TWP as an important *non-ENSO* source of skill over the U.S. during late fall may have been premature, for some of this skill could have been due to ENSO effects in the TWP region.

Finally, given the recent warming trend in the TWP (which does not affect our results), our findings may have implications for how the climate will be affected if the TWP region continues to warm and may suggest, in particular, that the effects be different in late fall than in winter.

REFERENCES

Alexander, M. A., 1992a: Midlatitude atmosphere–ocean interaction during El Niño. Part I: The North Pacific Ocean. *J. Climate,* **5,** 944–958.

——, 1992b: Midlatitude atmosphere–ocean interaction during El Niño. Part II: The North hemisphere atmosphere. *J. Climate,* **5,** 959–972.

——, and J. D. Scott, 1995: Atlas of climatology and variability in the GFDL R30S14 GCM. CIRES, University of Colorado, 121 pp. [Available from CDC/NOAA, R/CDC1, 325 Broadway, Boulder, CO 80305-3328.]

——, ——, and C. Deser, 2000: Processes that influence sea surface temperature and ocean mixed layer depth variability in a coupled model. *J. Geophys. Res.,* **105,** 16 823–16 842.

——, I. Bladé, M. Newman, J. R. Lanzante, N.-C. Lau, and J. D. Scott, 2002: The atmospheric bridge: The influence of ENSO teleconnections on air–sea interaction over the global oceans. *J. Climate,* **15,** 2205–2231.

Barsugli, J. J., and P. D. Sardeshmukh, 2002: Global atmospheric sensitivity to tropical SST anomalies throughout the Indo-Pacific basin. *J. Climate,* **15,** 3427–3442.

Bladé, I., 1999: The influence of midlatitude ocean–atmosphere coupling on the low-frequency variability of a GCM. Part II: Interannual variability induced by tropical SST forcing. *J. Climate,* **12,** 21–45.

Broccoli, A. J., and S. Manabe, 1992: The effects of orography on midlatitude Northern Hemisphere dry climates. *J. Climate,* **5,** 1181–1201.

Chen, T.-C., 2002: A North Pacific short-wave train during the extreme phases of ENSO. *J. Climate,* **15,** 2359–2376.

Deser, C., A. S. Phillips, and J. W. Hurrell, 2004: Pacific Interdecadal Climate Variability: Linkages between the tropics and North Pacific during boreal winter since 1900. *J. Climate,* **17,** 3109–3124.

Gordon, C. T., and W. F. Stern, 1982: A description of the GFDL global spectral model. *Mon. Wea. Rev.,* **110,** 625–644.

Hamilton, K., 1988: A detailed examination of the extratropical response to tropical El Niño/Southern Oscillation events. *J. Climatol.,* **8,** 67–86.

Hoerling, M. P., and A. Kumar, 2003: The perfect ocean for drought. *Science,* **299,** 691–694.

Huang, H.-P., R. Seager, and Y. Kushnir, 2005: The 1976/77 transition in precipitation over the Americas and the influence of tropical SST. *Climate Dyn.,* **24,** 721–740.

Kinter, J., C. K. Folland, and B. P. Kirtman, 2006: Workshop on climate of the 20th century and seasonal to interannual climate prediction. *CLIVAR Exchanges,* No. 11, International CLIVAR Project Office, Southampton, United Kingdom, 30–31.

Klein, S. A., B. J. Soden, and N.-C. Lau, 1999: Remote sea surface temperature variations during ENSO: Evidence for a tropical atmospheric bridge. *J. Climate,* **12,** 917–932.

Lau, N.-C., and M. J. Nath, 2003: Atmosphere–ocean variations in the Indo-Pacific sector during ENSO episodes. *J. Climate,* **16,** 3–20.

——, A. Leetmaa, and M. J. Nath, 2006: Attribution of atmospheric variations in the 1997–2003 period to SST anomalies

in the Pacific and Indian Ocean basins. *J. Climate,* **19,** 3607–3628.

Lindzen, R. S., and S. Nigam, 1987: On the role of sea surface temperature gradients in forcing low-level winds and convergence in the tropics. *J. Atmos. Sci.,* **44,** 2418–2436.

Livezey, R. E., M. Masutani, A. Leetma, H. Rui, M. Ji, and A. Kumar, 1997: Teleconnective response of the Pacific–North American region atmosphere to large central equatorial Pacific SST anomalies. *J. Climate,* **10,** 1787–1820.

Mo, K. C., and R. E. Livezey, 1986: Tropical–extratropical geopotential height teleconnections during the Northern Hemisphere winter. *Mon. Wea. Rev.,* **114,** 2488–2515.

Newman, M., 2007: Interannual to decadal predictability of tropical and North Pacific sea surface temperatures. *J. Climate,* **20,** 2333–2356.

——, and P. D. Sardeshmukh, 1998: The impact of the annual cycle on the North Pacific/North American response to remote low-frequency forcing. *J. Atmos. Sci.,* **55,** 1336–1353.

Palmer, T. N., and J. A. Owen, 1986: A possible relationship between some "severe" winters in North America and enhanced convective activity over the tropical west Pacific. *Mon. Wea. Rev.,* **114,** 648–651.

Quan, X., M. Hoerling, J. Whitaker, G. Bates, and T. Xu, 2006: Diagnosing sources of U.S. seasonal forecast skill. *J. Climate,* **19,** 3279–3293.

Seager, R., 2007: The turn of the century North American drought: Global context, dynamics, and past analogs. *J. Climate,* **20,** 5527–5552.

Simmons, A. J., J. M. Wallace, and G. W. Branstator, 1983: Barotropic wave propagation and instability, and atmospheric teleconnection patterns. *J. Atmos. Sci.,* **40,** 1363–1392.

Smith, T. M., and R. W. Reynolds, 2004: Improved extended reconstruction of SST (1854–1997). *J. Climate,* **17,** 2466–2477.

Trenberth, K. E., and J. W. Hurrell, 1994: Decadal atmosphere–ocean variations in the Pacific. *Climate Dyn.,* **9,** 303–319.

——, 1997: The definition of El Niño. *Bull. Amer. Meteor. Soc.,* **78,** 2771–2777.

Vose, R. S., R. L. Schmoyer, P. M. Steurer, T. C. Peterson, R. Heim, T. R. Karl, and J. K. Eischeid, 1992: The global historical climatology network: Long-term monthly temperature, precipitation, sea-level pressure, and station pressure data. Carbon Dioxide Information Analysis Center Tech. Rep. ORNL/CDIAC-53, NDP-041, Oak Ridge National Laboratory, 25 pp.

Wang, H., and R. Fu, 2000: Winter monthly mean atmospheric anomalies over the North Pacific and North America associated with El Niño SSTs. *J. Climate,* **13,** 3435–3447.